19 Isotope Production
for Medical Applications

A.D. Roberts[1,2,3], T.E. Barnhart[1], and R.J. Nickles[1]

[1] University of Wisconsin, Department of Medical Physics, Madison, WI, USA
[2] University of Wisconsin, Department of Psychiatry, Madison, WI, USA
[3] University of Manchester Molecular Imaging Centre, Christie Hospital, UK
   arobert5@facstaff.wisc.edu
   tebarnhart@wisc.edu
   rnickles@facstaff.wisc.edu

19.1 Introduction

The use of radiation for medical imaging and therapy has a long history, originating almost immediately in the earliest days of the X-rays discovered by W.C. Röntgen in 1895, and the subsequent discovery of natural radioactivity by Becquerel in 1896 and the separate isolation of radium by Pierre and Marie Curie in 1898. The use of radioactive materials was limited to natural radioisotopes until the demonstration of induced nuclear transformations using an accelerated beam by Cockcroft and Walton [1]. Despite the relatively widespread use of accelerators in the following decade for radioisotope production, these early machines were quite limited in the amount of useful radioactive material they could produce.

The field quickly evolved with the advent of nuclear reactors and improved charged-particle accelerators as part of the weapons programs in the Second World War. By far the most prolific source of man-made radioisotopes was from the energetic neutrons from nuclear reactors. While medical applications of these isotopes quickly evolved, the scarcity of reactor sources and the nature of neutron-induced reactions generally limited the field to the use of long-lived, neutron-rich nuclei. These isotopes and subsequent procedures are by far the most widely used in nuclear medicine today. There are numerous biological applications using reactor-produced radionuclides such as ^{14}C and ^{32}P. Medical applications include in vivo photon imaging (SPECT, single-photon-emission computed tomography) of source compounds labeled with ^{125}I, ^{99}Tc and many other isotopes. Other reactor-produced isotopes have found uses in radiotherapy, taking advantage of the local cell-killing capabilities of heavy-particle disintegration, particulary α-particles.

While the application of reactor-produced isotopes for medical purposes continues to be important, it was quickly realized that there are advantages to using accelerator-produced isotopes. First, the flexibility of using beams of well-defined energy allows for controlled selection of nuclear reactions. Next, the use of positively charged beams, typically of protons, deuterons or helium nuclei, allows the selective production of proton-rich radioisotopes, greatly

expanding the choice of isotopes available for medical use. More importantly, for imaging applications, radioisotopes can be produced in this manner with a change in proton number, facilitating easier chemical separation of the reaction products from the starting material. This can be crucial in the synthesis of compounds suitable for medical use, allowing complex radiochemistry to be performed, and efficient removal of the often toxic bulk material.

A further need for charged-particle-produced radioisotopes is in the imaging application of PET (positron emission tomography). Isotopes that decay by positron emission can be located using pairs of coincidence scintillators tuned to the characteristic $511\,\mathrm{keV}$ gamma rays emitted at near $180°$ upon positron–electron annihilation. By using rings of detector pairs, three-dimensional distributions of PET radioisotopes can be quantitatively imaged. In addition to the true three-dimensional distribution quantitation, there are significant advantages of using PET radioisotopes in medical studies, including the availability of chemical compounds labeled with naturally occurring light radioisotopes such as ^{15}O, ^{13}N and ^{11}C, and lifetimes well matched to the imaging requirements of physiological pathways of interest, seconds to hours rather than years.

While much of the early development work on isotope production originated out of nuclear-physics laboratories using electrostatic accelerators, most recent installations use commercially available small cyclotrons. The main beam requirements are energy and current, and the precise energy definition required for nuclear-physics experiments is less important. Nonetheless, isotope production with tandems still has a role in the field. The accelerator technology is well established, robust and comparatively inexpensive, and in some cases may be a matter of necessity, for example through collaboration with established physics or engineering tandem facilities. Furthermore, few commercial production cyclotrons allow much tuning of the beam shape and energy, hampering some basic development work on isotope production. Finally, most commercial cyclotrons require costly technological additions to provide different particle beams (protons vs. deuterons, typically), a feature readily available with the electrostatic tandem.

19.2 Historical Perspective

Since its initial development in the 1930s [2], the electrostatic accelerator, insulated under high pressure, has dominated the field of nuclear investigations. This was the direct result of the exquisite control of such beam variables as:

– energy, with an achievable resolution of $\delta E/E \approx 10^{-6}$ [3]
– geometry, with microbeams of μm dimensions [4]
– polarization [5, 6]
– heavy-ion capability, with the tandem today acting as the second accelerator in radioactive-ion-beam experiments [7].

Yet curiously, the electrostatic accelerator has seldom played a major role in radionuclide production for radiochemical or biological applications. This is due to a mismatch between the technical finesse of the machine and the brute needs of high currents on thick targets, analogous to pulling a plow with a thoroughbred. Cyclotrons arose as the more logical and reliable source of proton beams of $50\,\mu A$, 10–30 MeV, and have now evolved into near turnkey "black boxes" that almost disappear into the infrastructure that underlies a modern medical facility. This evolutionary path was shaped by the perceived beam current limitations of the tandem, a limitation that has been removed by today's multicusp negative-ion sources [8].

In the past, occasionally situations arose that exploited the tandem's advantages. A number of important radionuclides can be best produced by the irradiation of extremely costly, isotopically enriched targets. Examples of this include $^{78}Kr(p, \alpha)^{75}Br$ [9], $^{80}Kr(d, n)^{81}Br$ [10] and today's interest in making ^{124}I from enriched ^{124}Te. In cases where target material costs can reach many tens of US dollars/mg, a thick target (≈ 100 mg/cm^2) demands shrinking the diameter of both the beam and the target to the order of mm. In this application, the tandem excels with its tight beam emittance matched to miniature-target configurations [11].

A second application flexing the electrostatic tandem accelerator was an unsuccessful effort to make useful activities of radionuclides farther removed from beta-stability through heavy-ion reactions. As an instructive example, the $^{40}Ca(^{16}O, \alpha)^{52}Fe$ reaction invites the production of an important biological tracer without recourse to an isotopically enriched target or beam stock. In fact, the measured production rate was of the order of hundreds of Bq/(μA h) (RJN, unpublished data), disappointing even though it was performed parasitically in the Faraday cup of a "dues-paying" reaction study upstream. Heavy-ion reactions are poorly suited for the production of radiotracers simply because of the minuscule utilization of the beam. This utilization reaches nearly one ^{18}F nucleus created per thousand protons for the (p, n) reaction on ^{18}O at 11 MeV, but is drastically reduced by the Z^2 dependence of the stopping power of the ^{16}O beam, and the coupled problems of making beams of tens of μA of negative ions and stripping them to high charge states. Finally, the large number of competing exit channels saps the total reaction cross section above the Coulomb barrier, routing most of the flux into few-particle transfer reactions, resulting in products that could have been reached much more simply by a light-ion approach.

What has changed the landscape, in the seven decades since its birth, is the refinement of the tandem electrostatic accelerator into a reliable, high-current resource that rivals today's commercial cyclotron in almost every respect, save for compactness and familiarity within the radiochemistry community. The former limitation is site-specific, the latter amenable to education.

19.3 Isotope Production Physics

Regardless of the accelerator used, the first key to determining its applicability to production of a given radioisotope is an evaluation of the total reaction yield. Most common PET radioisotopes have had their yields measured over a variety of energies, but it can be useful to revisit these data, particularly in poorly documented cases or where novel radioisotopes are proposed. These calculations are particularly important when evaluating the use of linear accelerators, which most commonly have lower energies than comparably sized cyclotrons available today.

If the total reaction cross section is known, as is often the case for most isotopes used in medicine, the total reaction yield for a thin target can be calculated in the usual way. The nomenclature for the yield Y at a given energy is typically given in MBq/μA at saturation bombardment for short-lived isotopes (less than a few hours), and MBq /(μA h) for longer-lived isotopes.

Thin targets are rarely used in isotope production, particularly with lower-energy beams. The reaction of interest is typically the first channel available, for example (p, n) or (d, n), so to maximize yield the target material is thick enough to completely stop the beam. The details of the target thickness are sometimes difficult to determine, particularly in cases of gas targets that may see localized density reduction depending on the beam current and energy deposition. However, provided the target is truly thick and stops the beam at some unspecified point, the yield can be calculated using the well-known linear stopping power of the target material dE/dx. Published stopping-power data are quite sufficient for these calculations [12]. Equation (19.1) gives the calculated differential yield for a thick target. Integration over the appropriate energy range gives the total yield. The energy loss (dE/dx), the energy-dependent cross section (σ), the target density used for the energy loss (ρ) and the atomic weight (AW) are required for each calculation. The conversion factors give the reaction rate in MBq and the beam current in μA.

$$\frac{dY}{dE} = \left(\frac{dx}{dE}\right)\sigma\rho\left(\frac{6.02 \times 10^{23}}{AW}\right)\left(\frac{MBq}{10^{-6}\,s^{-1}}\right)\left(\frac{1}{1.6 \times 10^{-19}\,μA}\right)\left(\frac{1}{10^{6}\,s}\right)$$
(19.1)

As an example, several "standard" PET radioisotope yields have been calculated up to 10 MeV, as shown in Fig. 19.1. This is by no means a complete listing, but can serve in determining the applicability of a given accelerator to this task. Further discussion of these target systems is given in Sect. 19.5.2.
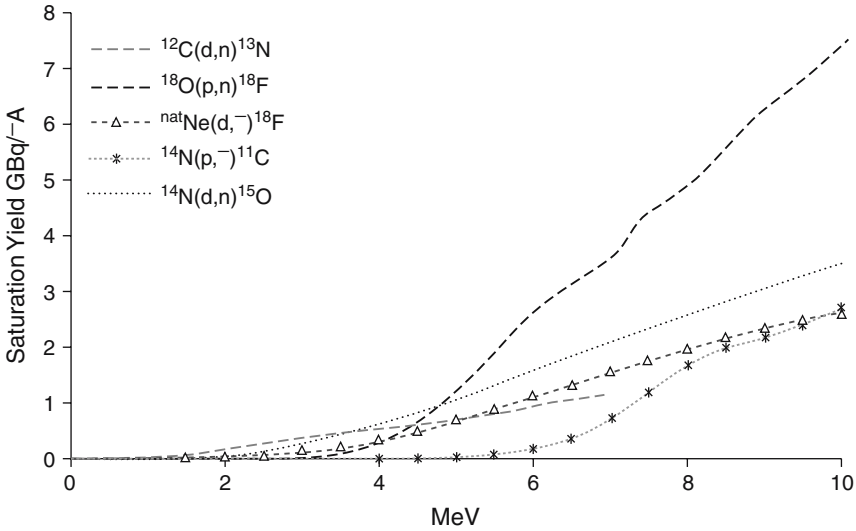
Fig. 19.1. Calculated thick-target saturation yields for some common PET radioisotopes [13]

19.4 Targetry Considerations

While total reaction yield is clearly important for radioisotope applications, there are several other considerations in developing production systems, particularly for medical applications.

By definition, a tracer imaging study requires a total mass of the material being tracked that does not itself perturb the physiological system studied. Therefore, it is crucial to maximize the specific radioactivity (SA) of the product, or the ratio of radioactive to nonradioactive tracer material. This is typically given in terms of GBq/μmol. Some studies require higher SA than others, clearly, and the targetry requirements can be adjusted accordingly. For example, an imaging study using a ^{11}C-labeled neuroreceptor ligand may require a starting source of ^{11}C with an $SA > 370\,\mathrm{GBq/\mu mol}$, while a simple ^{15}O-labeled-water study for flow may have no SA requirement to speak of.

Another consideration is radionuclidic purity. Impurities can interfere with the identification of the desired isotope activity and concentration, and, in the case of medical imaging, can cause problems with radiation dosimetry. In most cases, for PET applications, radioisotopic purity is not difficult to achieve. The low-energy beams used with tandem accelerators and the simplicity of the target materials rarely allow reactions other than the desired ones. In the case where other reactions are possible, or where the target composition presents alternate target nuclei to the beam, the radioactive impurities can usually be separated chemically, or in some cases of short

impurity half-life simply allowed to decay. Nonetheless, new systems must be monitored for impurities, and validated for their adequate removal.

Isotopes used in medicine are typically incorporated into some chemical form of physiological interest after production on the accelerator, so care must be taken to produce the isotope in an appropriate form to match the next step of chemical synthesis. For example, ^{13}N is readily made by low-energy deuteron irradiation of graphite, but the isotope is chemically trapped in the carbon matrix and not readily available for synthesis into a useful tracer form (e.g. ^{13}N-ammonia).

In addition to the correct chemical form of the radiotracer, care must be taken to minimize the amount of any stable chemical in the target material that could interfere with the subsequent chemistry. Using PET as an example again, one of the primary contaminants possible with aqueous ^{18}F-fluoride production is hydrocarbons. Trace amounts of ethanol, for example, can severely harm the downstream nucleophilic-substitution chemistry.

19.5 Examples of Isotope Production Systems

Every installation of an accelerator facility for medical radioisotope production will have its own unique requirements. While covering all possible contingencies is beyond the scope of this chapter, it can be useful to consider the specific example of a PET radioisotope production facility at the University of Wisconsin (UW), Madison. Much of the basic facility and targetry requirements met in this installation can serve as an example for what is needed elsewhere.

The Keck Laboratory for Functional Brain Imaging was created at the UW Waisman Center to provide a multidisciplinary resource for brain imaging and development studies. The lab, opened in early 2001, incorporates high-field MRI, high-resolution EEG, transcranial magnetic stimulation, and a full clinical and research PET facility.

Radioisotopes for the PET program are provided on site by an NEC 9SDH-2 tandem accelerator, purchased in 1996. The 9SDH-2 Pelletron was designed to provide $100\,\mu$A of 6 MeV protons or deuterons within a maximum 10 mm diameter beam spot. The actual performance regularly exceeds these specifications. The Torvis multicusp ion source typically achieves more than $150\,\mu$A [8]. The two chains, rated at $150\,\mu$A each, charge the high-voltage terminal, with demonstrated accelerated-beam currents in excess of $115\,\mu$A. The dome voltage of 2.97 MV required for 6 MeV single-charge beams (with a 50 keV ion source voltage) is conservative, and the accelerator has been run up to 3.48 MV (for a 7.0 MeV beam). The beam optics components include low-energy steering, and high-energy quadrupole focusing and steering magnets. The tuning capabilities, coupled with an in-line rotating-wire beam profile monitor, allow fine, continuous control of the beam shape and position. The

independent adjustment of beam width in two dimensions is typically from 6 to 10 mm, with a full practical range of 2 to 20 mm FWHM.

Although this machine is intended primarily for the continuous production of short-lived tracers labeled with ^{15}O ($t_{1/2} = 122$ s) or ^{17}F ($t_{1/2} = 65$ s), high-power target systems have been developed to provide [^{15}O] H_2O (yield at saturation 329 MBq/μA), [^{17}F] F_2 (936 MBq/μA), [^{18}F] fluoride (411 MBq/μA), [^{18}F] F_2 (370 MBq/μA), in-target production of [^{13}N] NH_3 (78 MBq/μA), [^{11}C] CO_2 (311 MBq/μA) and [^{11}C] CH_4 (303 MBq/μA).

Figure 19.2 shows the general layout of the tandem lab and the radiochemistry support facilities. Several points should be made that distinguish this layout from a typical nuclear-physics or engineering lab. First, this facility is intended for short-lived-radiotracer production. Placement of the accelerator close to the intended scanner is crucial. While some PET radioisotopes can be effectively transported from the production facility to the end-use point, many installations must also account for the fact that the staff responsible for the accelerator may also be involved in the radiochemistry and the actual performance of PET scan protocols. In the UW example, the decision was made to combine all the PET support activities in one location, thus minimizing staff requirements as well as the losses due to long transit times. The tandem vault is located immediately adjacent to both the radiochemistry labs and the PET scanner suite.
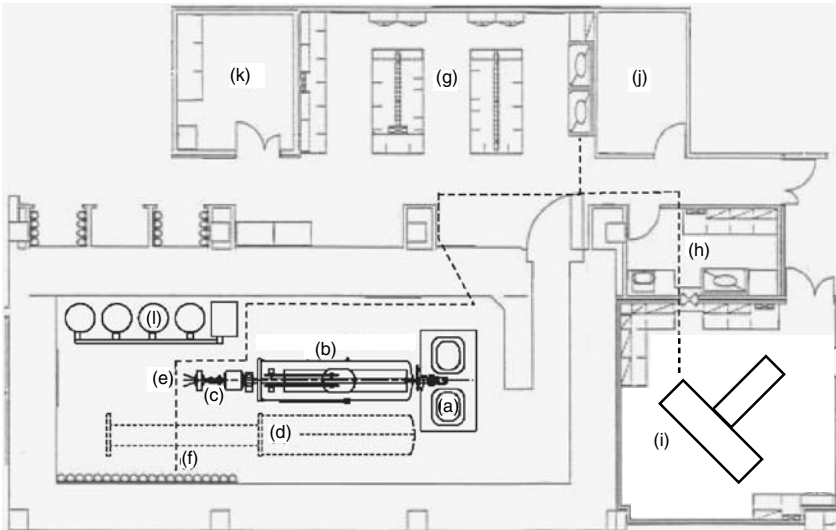

Fig. 19.2. Keck Laboratory radioisotope production and imaging area, including (**a**) Torvis ion source and control cabinets, (**b**) NEC 9SDH-2 accelerator, (**c**) focusing and switching elements, (**d**) accelerator position for maintenance, (**e**) target area, (**f**) gas supply lines, (**g**) lab area, (**h**) radiopharmacy, (**i**) PET scanner, (**j**) animal scanner and (**k**) machine shop

This lab arrangement puts rather stringent requirements on the radiation shielding, primarily for the neutrons resulting from (p, n) and (d, n) reactions during irradiation. While much can be achieved with localized shielding around the target areas, the UW installation went with a complete accelerator vault. The walls are standard concrete, >1.8 m thick all around. Care was taken to prevent direct neutron shine through any of the service access ports, with significant bends placed in the largest penetrations for air handling to ensure no leakage. The door is shielded from the target area by a dry-stacked wall of cement blocks, and is constructed of boron-impregnated high-density polyethylene backed by lead for stopping the neutron-capture gamma rays.

In total, the shielding and safety requirements for a medical installation are a significant cost, comparable to the accelerator cost itself. The source radiation can be significantly higher than that found in most nuclear-physics installations, and there is the added complication of shielding for the general public (e.g. PET scan subjects), sensitive local equipment (e.g. the PET scanner and other nuclear detection equipment) and the radiation workers themselves.

Shielding of personnel from the product radionuclide dose is obviously essential. In the case of PET radioisotopes, it is not uncommon to start with >100 GBq of activity produced. The primary shielding consideration is the 511 keV gamma ray dose, since the direct positron energies are typically < 2 MeV and easily shielded. Often the material is transported around a laboratory, from the accelerator target to chemistry stations to scanners, and must be handled appropriately at all points. The radioactive product is delivered via small-bore stainless steel or Teflon tubing from the target end of the accelerator, through a conduit in the shield walls, to a lead-lined trenching system leading to shielded chemistry stations or directly to the PET scanner. Table 19.1 lists the shielding characteristics for various materials, which can serve as a guide for analyzing transport lines, trenches etc. The gamma transmission drops exponentially with distance. Distance is also an effective means of minimizing dose rates. Equation (19.2) gives the dose rates measured for ^{18}F in air, at a distance d from the source:

$$\text{Dose rate} = 0.163 \frac{\mu\text{Sv m}^2}{\text{MBq h}} d^{-2} \tag{19.2}$$

Table 19.1. Shielding characteristics for various materials for 511 keV gamma rays. The fraction penetrating drops exponentially with thickness as $\mathrm{e}^{-\mu d}$

Material	μ (cm^{-1})
Lead	1.54
Steel	0.41
Cement	11
Glass	12

19.5.1 Target Entrance Windows

The UW installation was primarily designed for the shorter-lived PET radioisotopes, e.g. ^{15}O, although several standard and nonstandard medical isotopes have been produced with the NEC 9SDH-2 tandem. Most of the systems were based on existing PET targetry developments, and several excellent summary texts have been published on the field, e.g. [14, 15].

   One of the primary concerns with radioisotope production common to most targetry systems is the proper handling of the beam power. The total beam power is linear with current and energy, typically on the order of 1 kW or more. This amount is not typically problematic, and simple water cooling of the target body material is generally sufficient, with examples shown for the targets discussed below. When one is using lower-energy beams, typical of most electrostatic-accelerator installations, special consideration is necessary to take to account of the increase in linear energy loss in the target windows. Liquid, gas and some volatile solid targets require thin windows to separate the target material from the beamline vacuum. Given the typical low yields for lower-energy beams, these target windows must be thin to preserve the available energy. Figure 19.3 shows the energy dependence of the beam energy loss in two common entrance-window foils, Havar and aluminum. These windows must be thick enough to withstand the pressure without rupture.
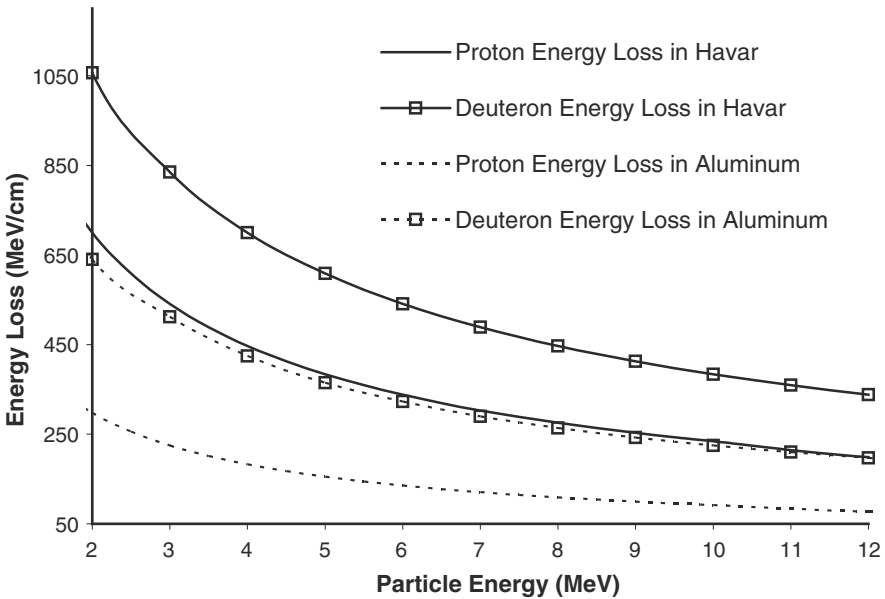

Fig. 19.3. Energy loss of protons and deuterons in aluminum and Havar

One solution to the problem of sealing a pressurized target volume to a vacuum system was provided by the method of the double-foil helium-cooled window [16]. This is a method that has been successfully used for radioisotope production with electrostatic accelerators [17]. An alternative and in some cases improved method has been reported [18, 19], employing a single thin window supported by a high-transmission grid. Gridded windows are now the preferred choice for radioisotope production targets for the UW 3 MV electrostatic tandem accelerator. The removal of one target window foil reduces the energy loss, and the low beam emittance allows the use of deep grids and efficient water cooling [20].

The support grid pattern consists of circular holes arranged in a hexagonal pattern. Trials were done with differing-size holes to maximize the allowable beam current. Figure 19.4 shows the basic design of this grid, with 80 holes of 1.7 mm diameter. The grid is constructed from a single aluminum unit, incorporating water cooling for maximum heat transfer with no material discontinuities. The deep grid holes provide increased material for heat transfer to the water cooling with negligible loss of the near-parallel beam. The aluminum was machined to a minimum wall thickness of 0.18 mm between the holes, with a grid depth of approximately 12.5 mm along the beam path. Deeper grid holes up to 25 mm deep have been used with no change in performance with the tandem accelerator. The targets for the tandem accelerator had the grid holes arranged to cover a $2.85\,\text{cm}^2$ area to minimize the heating of the grid. The grids are water-cooled through two straight channels on opposite sides of the support grid. Chilled water at 18°C flows at 2.3 l/min through the cooling channels of the grid. The support grid mounts onto the beamline with a KF-40 quick-connect flange. Single entrance-window foils have been tested with thicknesses ranging from 12.7 to 25.4 µm aluminum and 2.5 to 12.7 µm Havar.

Limitations of the water-cooled support grid have been found from foil failures occurring at high beam currents with narrower beam profiles. Typically the beam profile of 6 MeV deuterons is run at 8 mm FWHM in both directions, but when the beam profile is changed to a narrower 5.5 mm FWHM in both directions, 25.4 µm aluminum foils fail at above 70 µA (by developing
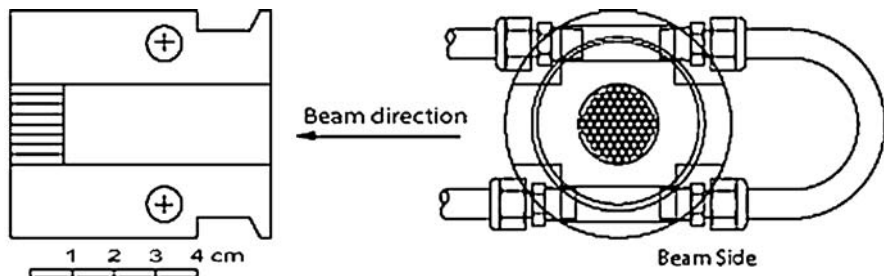

Fig. 19.4. Basic schematic of standard water-cooled support grid
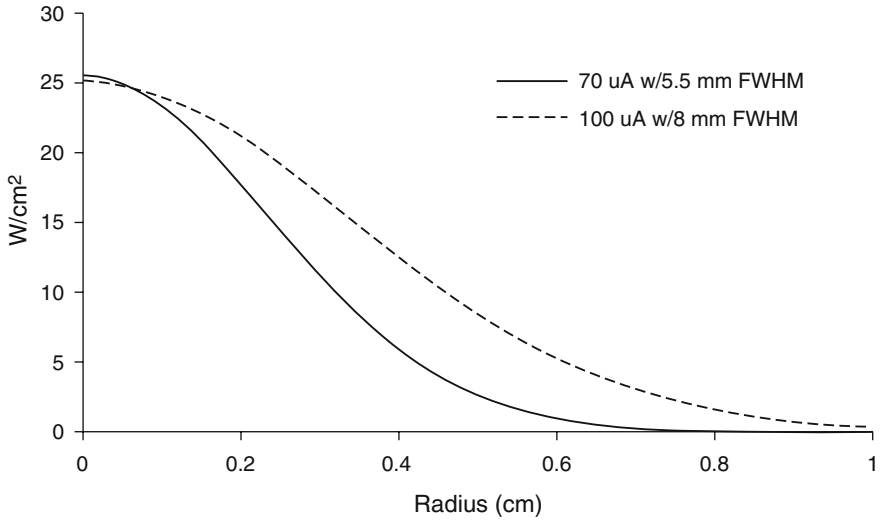
Fig. 19.5. Maximum power on a 1.6 mm diameter hole grid vs. beam profile on a 25 μm aluminum entrance window [20]

pinholes). Figure 19.5 shows the energy deposition from 6 MeV deuterons in 25.4 μm aluminum foil for both 70 μA 5.5 mm FWHM and 100 μA with 8 mm FWHM, assuming Gaussian profiles. From the plot, the energy per unit area is higher for the 70 μA with beam at the center; above this energy, the foils fail. The 100 μA beam is lower at the center, and without the resulting failures. This demonstrates the upper limit on the energy per unit area for these foils on grids with 1.7 mm diameter holes. This could also be used to estimate the performance with higher-energy protons and deuterons of the water-cooled support grid.

Optimization of the hole size was performed by calculation of the maximum current density on the target material. The peak current of the beam profile at the maximum allowable beam current on a particular grid gives the maximum current density on the grid. Estimation of the maximum current density on the grid for holes smaller than those constructed was performed by a least-squares fit of the known maximum current densities for the various grid sizes, including the maximum current density for an unsupported single-foil target window. The transmission for all grids was estimated under the constraint of a consistent minimum wall thickness of 0.18 mm, which is reasonable for fabrication by standard or wire-electron-discharge machining, with 0% transmission for infinitely small grid holes and 100% transmission for an unsupported window. The product of the transmission and the maximum beam current density on the grid is the maximum current density on the target material. Figure 19.6 shows the maximum current density on the target material vs. the grid hole size, using 25.4 μm aluminum target windows. The
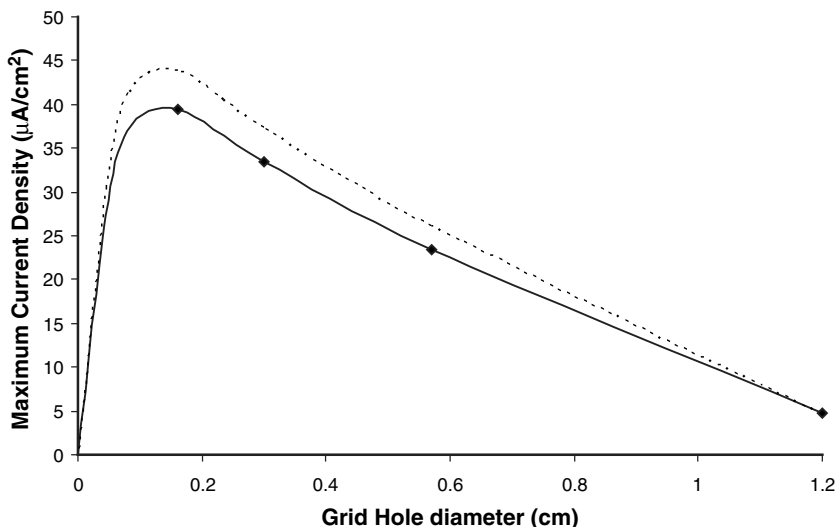
Fig. 19.6. Maximum current density ($\mu A/cm^2$) on the target material vs. grid hole diameter. In each case a minimum amount of material between holes of thickness 0.18 mm is assumed. The maximum current density is the product of the grid transmission fraction and the measured maximum allowable peak current density ($\mu A/cm^2$). Points (black dots) correspond to the measured maximum beam current with a 25.4 μm aluminum window at $\leq$350 kPa on a flow-through gas target. The dashed curve is the estimated improvement in maximum current density if it is corrected for the improved transmission with hexagonal holes [20]

points correspond to the measured maximum beam current density and the grid hole size. The solid curve represents the estimations obtained from the measurements down to smaller grid hole diameter. The optimum point for maximum current density on the target material lies near the smallest grid hole diameter tested, below which the grid transmission loss dominates the maximum current density at smaller hole sizes.

Hexagonal grid holes have been proposed as a means of improving the in grid transmission [21, 22]. The improvements in grid performance obtained by using hexagonal holes instead of circular holes can also be calculated from the maximum current density on the target material. The improvement in transmission by the reduction of material is approximately 12%. Figure 19.6 shows the improvement in the maximum current density on the target material as a dashed curve above the calculation for circular holes.

19.5.2 Examples of Production Targets

Oxygen-15 ($t_{1/2} \sim 2\,\text{min}$)

Oxygen-15 is one of the earliest radioisotopes used for PET studies, and continues to be used for studies of fast processes such as blood flow, using primarily [^{15}O] water but in some cases [^{15}O] butanol or other freely diffusible compounds. It has also been used directly in the form of [^{15}O] O_2 gas for tissue oxygen utilization measurements, as well as [^{15}O] CO and CO_2 for blood volume and flow measurements, respectively. The simplest reaction to use is ^{14}N(d, n)^{15}O, taking advantage of both the high yields at low energy and the economical use of the natural isotopic abundance of the target material. Gas targets are used, typically with 99% N_2 gas and an admixture of an appropriate gas to form the required chemical product. In the case of [^{15}O] water, hydrogen is used as the mix gas. Similarly, replacing the hydrogen with oxygen produces [^{15}O] O_2.

   Figure 19.7 shows the typical gas target used for ^{15}O systems. The target body is aluminum, a preferred material for many systems owing to ease of fabrication, high thermal conductivity, and low residual radiation activation from stray-beam impact. The gas chamber of the target body is 19 mm in diameter and 127 mm in length, with the outside diameter of the target being ∼50 mm. The 25 μm aluminum target window is supported with the cooled grid as discussed.
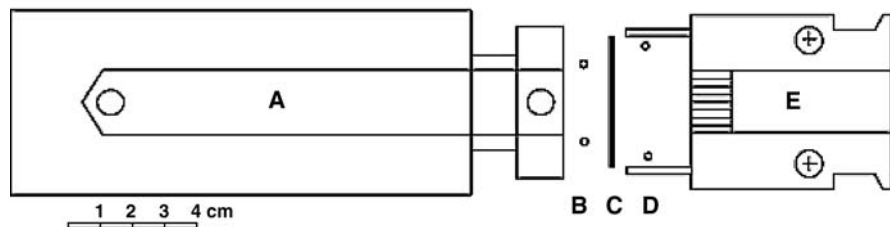

Fig. 19.7. Typical ^{15}O gas target assembly. (**A**) is the T-6061 aluminum gas target body, with a 19 mm i.d. and 127 mm length bore; (**B**) and (**D**) are Viton O-rings; (**C**) is the aluminum entrance foil; and (**E**) is the water-cooled support grid

   Typical operation parameters for in-target [^{15}O] water production use a flow-through technique. 350–700 kPa of premixed N_2/1%H_2 fills the gas target body and flows to the chemistry area at a flow rate of 200–400 cm^3/min. A lower target pressure allows reasonable gas flow rates in the collection vials without the use of metering or needle valves in the gas stream. As all fittings and valves in the gas stream collect and condense the [^{15}O] water, reducing the yield collected from the target, a minimum should be used between the target and the collection area. The beam current for [^{15}O] water production

is usually between 10 and $20\,\mu A$. Irradiation and collection last for about $2–4\,min$, minimizing the amount of NH_3 produced. Collection of the activity for the study results in $>4\,GBq$ of $[^{15}O]$ water, of which 350 to $2500\,MBq$ is injected.

Unlike $[^{15}O]$ water, $[^{15}O]$ O_2 does not stick to the target and the lines coming from the target to the chemistry hood. This target is generally shot as a static target and dumped in a reservoir with a minimum (reasonable) volume for inhalation. The target pressures are higher, $\sim650\,kPa$, and take advantage of the full thick-target yield. The beam current for $[^{15}O]$ O_2 production is similar to that for $[^{15}O]$ water, at $10–20\,\mu A$ for oxygen utilization studies. Irradiation times for O_2 production are usually about $4–5\,min$. These preparations generally result in $>10\,GBq$ of $[^{15}O]$ O_2.

Carbon-11 ($t_{1/2} = 20\,min$)

Carbon-11 has been widely used for the labeling of novel research tracers for PET. The half-life is long enough to probe more complex physiological parameters, such as specific binding of radioligands to neuroreceptors. The fact that it is carbon means complex molecules can be turned into PET tracers with no chemical differentiation from the cold compound. This is particularly important when one wants to use PET to follow the tracer kinetics of labeled drugs at subpharmacological levels without affecting the behavior of the drug.

Several avenues have been explored for ^{11}C production; these include $^{11}B(p, n)^{11}C$ and $^{14}N(p, \alpha)^{11}C$. The first provides reasonably high yields at low energy, but requires the use of solid targets, typically boron oxide, and subsequent extraction of ^{11}C for chemical use. The gas phase production with $^{14}N(p, \alpha)^{11}C$ suffers from a lower yield; however, it can greatly simplify the subsequent chemistry.

^{11}C is typically produced in the form of CO_2 or methane (CH_4). The basic system is identical to that for ^{15}O production, in that the target gas is primarily natural nitrogen, with a small admixture of an appropriate balance gas to produce the desired product. In the case of $[^{11}C]$ CO_2, the mix is $<1\%$ oxygen, while for methane, a higher mix of hydrogen is optimal, on the order of 10%.

The UW $[^{11}C]$ methane target is machined from stainless steel rather than aluminum. The cylindrical gas chamber has a $19\,mm$ diameter and a $135\,mm$ length. Unlike the aluminum gas targets, which have good thermal conductivity, the stainless steel target requires a water jacket that is TIG welded to the target body at the front and rear. The gas stream enters at the rear of the target and leaves at the front on the mounting flange. A water-cooled support grid secures and cools the entrance window (Havar).

In-target $[^{11}C]$ methane is produced using a static shot technique. The target pressure inside the stainless steel gas target body is increased to $1\,MPa$ for this reaction, as the protons have a longer range than deuterons. The

increased pressure also compensates for the reduced nitrogen and the reduced target thickness arising from the premixed $N_2/10\%H_2$. The beam current for [^{11}C] methane production is usually between 50 and 100 μA at 6.8 MeV, with a yield of 303 MBq/μA.

Fluorine-18 ($t_{1/2}$ = 110 min)

While ^{11}C has some clear advantages for producing PET tracers identical to many known drugs or natural compounds, the short half-life does limit its potential for widespread distribution. Also, some physiological processes may require longer times to reach equilibrium, requiring scans of 1–2 h to interpret fully.

The main reaction channels available with low-energy beams are ^{18}O(p, n)^{18}F and ^{20}Ne(d, α)^{18}F. With higher-energy machines (>10 MeV), the yield advantage for the ^{18}O(p, n)^{18}F reaction is quite substantial (see Fig. 19.1) and most target systems use the expensive isotopically enriched ^{18}O, in the form of either water or oxygen gas. While these systems have been used successfully with tandem accelerators [17, 23], the yield advantage compared with the neon target is diminished, and allows the use of natural neon, with no costly isotopic enrichment.

^{20}Ne(d, α)^{18}F, for [^{18}F]F_2 Production

Two systems for ^{18}F production using ^{20}Ne(d, α)^{18}F are in use at UW. The first system produces low-specific-activity [^{18}F] fluorine gas (F_2). The basic methodology has been widely used in PET [24–27], producing ^{18}F-labeled compounds such as [^{18}F] fluoroDOPA for Parkinson's disease research.

[^{18}F] F_2 is produced in an aluminum-body gas target chamber similar to the ^{15}O system, although some institutions use nickel or stainless steel targets to minimize reactions of fluorine with the walls. The target gas is natural neon, with a nominal 0.5% cold fluorine. Using a 6 MeV deuteron beam with the tandem accelerator, the UW target produces [^{18}F] F_2 at a saturation yield of 370 MBq/'μA at 100 μA. The target can be run in a continuous-flow or a static mode, although in the flow mode care must be taken not to exceed the maximum fluorine load capacity of the downstream chemistry (typically <100 μmol of F_2 for most preparations).

^{20}Ne(d, α)^{18}F, for Aqueous [^{18}F] Fluoride Production

The low specific activity from the gas system above limits its use for medical applications. Where high specific activity is required, the ^{18}F can be extracted in the form of aqueous fluoride, with no addition of cold fluorine. This is the approach most commonly used in PET, and is the direct result of proton irradiation of [^{18}O] H_2O targets. However, one can still explore the production of no-carrier-added fluoride using the neon gas targetry, at a significant saving

in target materials compared with enriched ^{18}O. In the pure neon gas system, the ^{18}F ions drift to the walls of the target chamber and stick. The ^{18}F can then be washed off the walls with water, resulting in aqueous [^{18}F] fluoride. In this system, the wall material and treatment can have a dramatic effect on the performance of the system. Several groups have studied empirically the use of different materials for similar wash-off systems [23, 28–30]. While there is still some debate as to the exact mechanisms involved, some common results are beginning to emerge. Niobium seems to be well suited to use with fluoride systems, both for direct fluoride from [^{18}O] water and for our indirect wash-off target using the neon reaction.

The gas target for the production of [^{18}F] fluoride via the ^{20}Ne(d, α)^{18}F reaction varies from the other gas targets. The aluminum target body has been nickel-plated, and a niobium tube (15.7 mm I.D.) is inserted in the bore of the target. Holes drilled in the niobium tube align with the gas ports at front and rear, and with a third port centered on the bottom of the target, to drain the water wash. Water is preheated to 85°C, and kept hot through the washing process with heat tape wrapped around the target. The total water volume is approximately 20 ml per wash. Water washes of the interior surface of the gas target have given yields of 407 MBq/μA at 85 μA.

$^{18}O(p, n)^{18}F$, for Aqueous $[^{18}F]$ Fluoride Production

Liquid target systems have been developed for production of [^{18}F] fluoride from ^{18}O(p, n)^{18}F using enriched water targets with electrostatic tandem accelerators [17,30,31], as well as with most medical production cyclotrons (see e.g. [32]). The volume of the liquid target is generally kept low to minimize the use of enriched isotopes. The target cooling is more critical as hundreds of watts are usually imparted into less than 1 ml of liquid. The target pressure in a sealed system increases with the temperature of the liquid as it turns to vapor. Poisons from the target chamber can also detrimentally affect the chemistry post-irradiation. In the case of ^{18}F, aluminum cannot be used as a target body, since it not only binds the [^{18}F] fluoride, but also poisons radiosyntheses. For this reason, silver, niobium or titanium is a better alternative.

Figure 19.8 shows a schematic drawing of the simple high-pressure, silver-body target used on the UW tandem. The water delivery lines are Teflon or HPLC (high-pressure liquid chromatography)-grade stainless tubing (0.8 mm I.D.). The switch valves at the target are manual stainless steel ball valves with Teflon packing (Whitey, 40 series). The target body is silver, with stainless steel tubing top and bottom for water loading. The tubing is close-fit to the silver, and then silver-soldered in place. The cylindrical beamstrike volume is 12.7 mm O.D. by 3 mm deep, sufficient to stop 6 MeV protons in water. The beamstrike volume is 380 μl, with a total of 500 μl required to fill between the switch valves. The target mounts onto the water-cooled support grid, similar in design to the one used for the gas target, with the window
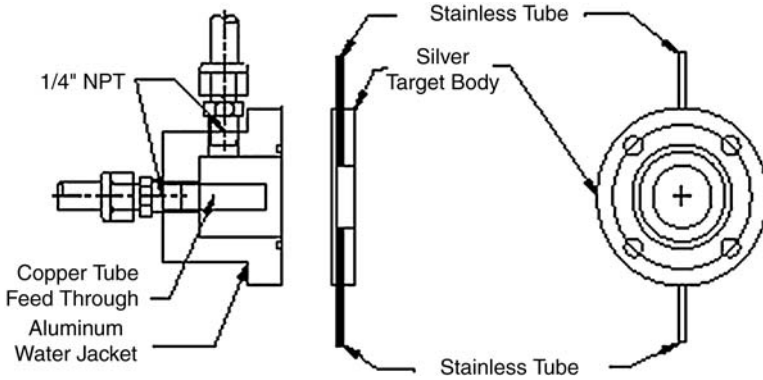
Fig. 19.8. Design of the UW ^{18}O water target

foil compressed against a Teflon O-ring. A water jet at the back of the body cools the target. 6.0 MeV protons irradiate the water through 12.7 µm Havar. The beam profile is kept to a maximum of 6 mm FWHM on the water target. While the reaction yield at ∼6 MeV is significantly less than that for higher-energy machines, several GBq of useful ^{18}F can be produced, sufficient for research PET purposes.

References

1. J.D. Cockroft, E.T.S. Walton: Proceedings of the Royal Society A, **136**, 619 (1932)
2. R.G. Herb: IEEE Transactions, **NS-30**(2), 1359 (1995)
3. S.E. Arnell: Nuclear Physics, **24**, 500 (1961)
4. G.M. Klody, J.B. Schroeder, J.A. Ferry, T.J. Pollock, E.D. Adams, R.G. Herb: Nuclear Instruments and Methods in Physics Research, **56–57**, 704 (1991)
5. W. Haeberli, W. Gruebler, P. Extermann, P. Schwandt: Physical Review Letters, **15**(6), 267 (1965)
6. W. Haeberli, M.D. Barker, C.A. Gossett, D.G. Mavis, P.A. Quin, J. Sowinski, T. Wise, H.F. Glavish: Nuclear Instruments and Methods in Physics Research, **196**, 319 (1982)
7. K.E. Rehm, M. Paul, A.D. Roberts: Nuclear Physics A **616**, C115 (1997)
8. M.L. Sundquist, J.R. Adney, R.C. Schmidt: Nuclear Instruments and Methods B **99**, 684 (1999)
9. A.M. Friedman, O.J. DeJesus, P. Harper, et al.: Journal of Labeled Compounds and Radiopharmaceuticals, **19(11-1)**, 1427 (1982)
10. P.V. Harper, B. Rich, K.A. Lathrop, B. Mock: Early Electrostatic Accelerators and Some Later Developments, IEEE Transactions, Report for the ID Atomic Energy Commission, IAEA-SM-185, P. 14 (1974)
11. R.J. Nickles, M.E. Daube, G.D. Hutchins: Journal of Labeled Compounds and Radiopharmaceuticals, **11**, 1365 (1983)
12. J.F. Janni: Atomic Data and Nuclear Data Tables, **27**, (1982)

13. S.M. Qaim, F.T. Tarkanyi, P. Oblozinsky, K. Gul, A. Hermanne, M.G. Mustafa, F.M. Nortier, B. Scholten, Y. Shubin, S. Takacs, Y. Zhuang, IAEA-TECDOC-1211, May 2001
14. J.C. Clark, P.D. Buckingham: *Short-Lived Radioactive Gases for Clinical Use.* Butterworths, London, 1975
15. G. Stöcklin, V.W. Pike: *Radiopharmaceuticals for Positron Emission Tomography.* Kluwer Academic, Dordrecht, 1993
16. B.W. Wieland: Proceedings of the First Workshop on Targetry and Target Chemistry, Heidelberg, pp. 14–16 (1985)
17. T. Ohlsson, A. Sandell, R. Hellborg, K. Håkansson, C. Nilsson, S.E. Strand: Nuclear Instruments and Methods in Physics Research A, **379**, 341 (1996)
18. R.J. Nickles: Nuclear Instruments and Methods in Physics Research A, **177**, 593 (1980)
19. D.J. Schlyer, M.L. Firouzbakht, I. Garcia, R.A. Ferrieri: Application of accelerators in research and industry, AIP Conference Proceedings 392, p. 1363 (1997)
20. T.E. Barnhart, A.K. Converse, K.A. Dabbs, R.J. Nickles, K.R. Buckley, S. Jivan, T.J. Ruth, A.D. Roberts: Water-cooled grid support system for high power irradiation with thin target windows, submitted to Applied Radiation and Isotopes **58** (1) pp. 21–26, 2003
21. G. Bida, R.E. Ehrenkaufer, A.P. Wolf, J.S. Fowler, R.R. MacGregror, T.J. Ruth: Journal of Nuclear Medicine, **21**, 758 (1980)
22. J.A. Nye, D.W. Dick, R.J. Nickles: 17th International Conference on the Application of Accelerators in Research and Industry, Denton, TX, AIP Conference Proceedings 680, P. 1098 (2002)
23. T.E. Barnhart, R.J. Nickles, A.D. Roberts: 17th International Conference on the Application of Accelerators in Research and Industry, Denton, TX, AIP Conference Proceedings 680, P. 1086 (2002)
24. G. Bida, B.W. Weiland, J. Lenz, C. Alvord: Proceedings of the Ninth International Workshop on Targetry and Target (Chemistry, Turku, Finland, pp. 24–29, May 23–25 2002)
25. G. Blessing, H.H. Coenen, K. Franken, S.M. Qaim: Applied Radiation and Isotopes, **37**, 1135 (1986)
26. V. Casella, T. Ido, A.P. Wolf, J.S. Fowler, R.R. MacGregror, T. Ruth: Journal of Nuclear Medicine, **21**(8), 750 (1980)
27. B.W. Wieland, D.J. Schlyer, A.P. Wolf: International Journal of Applied Radiation and Isotopes, **35**, 387 (1984)
28. F. Helus, V. Uhlir, G. Wolber, H. Gasper, W. MaierBorst: Journal of Radioanalytical and Nuclear Chemistry, **182**, 445 (1994)
29. T.J. Ruth, K.R. Buckley, K.S. Chun, E.T. Hurtado, S. Jivan, S. Zeisler: Applied Radiation and Isotopes, **55**, 457 (2001)
30. R.J. Nickles, R.D. Hichwa, M.E. Daube, G.D. Hutchins, D.D. Congdon: International Journal of Applied Radiation and Isotopes, **34**, 625 (1983)
31. A.D. Roberts, R.J. Davidson, R.J. Nickles: 15th International Conference on the Application of Accelerators in Research and Industry, Denton, TX, AIP Conference Proceedings 475, p. 106 (1998)
32. M.R. Kilbourn, P.A. Jerabek, M.J. Welch: International Journal of Applied Radiation and Isotopes, **36**, 327 (1985)